$\mathbf{R}_h = ct$ *Universe*

Malin Ouyang,[1,*] SiRui Ge,[1,†] and TianCheng Lu[1,‡]

[1] *The School of Astronomy and Space Science, Nanjing University, China*

I. INTRODUCTION

Modern cosmology, based on the FLRW metric [1], which is well-known solution to Einstein's equations, gives no guidance concerning the equation of state, $p = \omega\rho$ in the cosmic fluid. The standard model partitions the total energy density ρ and total pressure p into three primary components[2]: matter ρ_m, radiation ρ_r, and an unknown dark energy ρ_{de}, which is assumed to be a cosmological constant in ΛCDM model with $\omega_\Lambda = -1$. For the others, the standard model assumes that $\omega_m = 0$ and $\omega_r = -\frac{1}{3}$.

However, the standard model of cosmology is today confronted with several inconsistencies and unpalatable coincidences even though it represents the most successful attempt at accounting for the cosmological observations. For example, the Hubble tension has emerged as a major challenge in modern cosmology, reflecting a persistent discrepancy between measurements of the Hubble constant (H_0) from early-Universe observations and late-Universe distance ladder methods. While measurements of the cosmic microwave background (CMB) through the ΛCDM framework have converged to a value of $H_0 \sim 67 - 68\mathrm{kms}^{-1}\mathrm{Mpc}^{-1}$, late-Universe probes such as Cepheid-calibrated Type Ia supernovae consistently yield $H_0 \sim 73 - 74\mathrm{kms}^{-1}\mathrm{Mpc}^{-1}$. This $4-6\sigma$ discrepancy has intensified over the past decade as observational techniques have improved and systematic uncertainties have been rigorously examined. Proposed resolutions span modifications to the standard cosmological model, including early dark energy scenarios, evolving dark energy models, and interacting dark matter-radiation frameworks, while other investigations focus on potential systematics in distance ladder measurements or CMB interpretation[3].

The similarity with the ΛCDM model is found in the apparent equivalence between the Hubble horizon $R_h(t_0)$ and the distance ct_0, which is the distance light has traveled since the Big Bang, representing the presumed current age t_0 of our universe. This equivalence was initially noted as an anomaly of the standard model by Melia[4] and has been subjected to increased scrutiny over the past decade [5, 6], often referred to as the "zero active mass universe" or "$R_h = ct$ universe".

The $R_h = ct$ universe can be classified as an FLRW cosmology, characterized by a comparable distribution of energy components within the cosmic fluid. However, it advances further by adhering to the zero active mass condition as stipulated by general relativity, thereby imposing the constraint on the total equation of state to satisfy $\rho + 3p = 0$[5–7]. This stipulation seems necessary for the consistent application of the FLRW metric. According to the comparative analysis of the $R_h = ct$ and ΛCDM models as examined by Melia [8], it has been observed that over 30 distinct data sets indicate a preference for the $R_h = ct$ model, with a likelihood exceeding 90%, compared to approximately 10% for the ΛCDM model (refer to Table 2 in [8]). Although predictions from the ΛCDM model frequently approximate those of the $R_h = ct$ model, as illustrated in Figure 1, this convergence is confined to the far right side of the graph, particularly for values of $t \gtrsim 10^{15}s$. This analysis is grounded in the age-redshift relation within the ΛCDM framework, utilizing the expression

$$t^{\Lambda\mathrm{CDM}}(z) = \frac{1}{H_0}\int_z^\infty \frac{du}{\sqrt{\Omega_\mathrm{m}(1+u)^3 + \Omega_\mathrm{r}(1+u)^4 + \Omega_\Lambda}} \tag{1}$$

where, we keep in the basic assumption of a flat universe($k = 0$) and dark energy in the form of a cosmological constant, we have $\Omega_A = 1 - \Omega_m - \Omega_r$. The corresponding expression for $R_h = ct$ is

$$t^{R_\mathrm{h}}(z) = \frac{1}{H_0(1+z)} \tag{2}$$

As demonstrated in [9], the two trajectories derived from Equation 1 for $t \gtrsim 10^{-37}$s, along with $a(t) \propto e^{H_{inf}t}$ during the inflationary phase for the ΛCDM model (where H_{inf} signifies the constant Hubble parameter), and from Equation 2 for $R_h = ct$, unveil several fascinating correlations between these models. This comparison suggests that the optimized ΛCDM cosmological distances and expansion dynamics might simply replicate the characteristics of the more fundamentally derived model with $\omega = -\frac{1}{3}$.

The plot illustrates that, although it is possible to replicate $R_h = ct$ with ΛCDM for $z \lesssim 8$ by selecting suitable parameter values, this method increasingly fails as the expansion history is considered at earlier epochs. Specifically, the $R_h = ct$ model does not encounter temperature or electroweak horizon issues[8, 10], whereas ΛCDM necessitates inflation at $t \sim 10^{-37}$ seconds to account for the Universe's current state[11].

Even so, the complicated history of acceleration and deceleration applied to the standard model produces an overall expansion today exactly equal to what it would have been in $R_h = ct$ anyway. This is the motivation of the $R_h = ct$ model,i.e., the coincidence that our universe

* 221840237@smail.nju.edu.cn
† 221840089@smail.nju.edu.cn
‡ 221840117@smail.nju.edu.cn

today has an apparent horizon R_h exactly equal to ct. These relationships result in an equivalent present-day age of the Universe for both models (refer to fig.1), yet, at $z \gtrsim 6$, where the expansion factor is approximately $1/7$ (given $a_0 = 1$), t^{R_h} is approximately double that of t.

The article is structured as follows: Section II outlines the fundamental characteristics of the $R_h = ct$ universe, focusing on its derivation from the FRW equations(Section II A), the consequences drawn from Birkhoff's theorem(Section II B), and the characterization of the cosmic horizon R_h(Section II D). Section III gathers observational data in support of the model, including luminosity distance assessments(Section III A), high-redshift galaxy and quasar observations sourced from the JWST(Section III B), and constraints on the dark energy equation of state (ω_{de}) along with matter density (Ω_m)(Section III C). Section IV provides a critical analysis of ongoing challenges, such as the conflict between matter composition and the model's linear expansion dynamics, the timeline for the formation of supermassive black holes(Section IV A), and the inconsistencies with observed cosmic acceleration(Section IV B). In Section V, these discussions are synthesized, evaluating the explanatory potential of the $R_h = ct$ model in light of its theoretical and observational constraints, while positioning it as a possible alternative to the ΛCDM model.

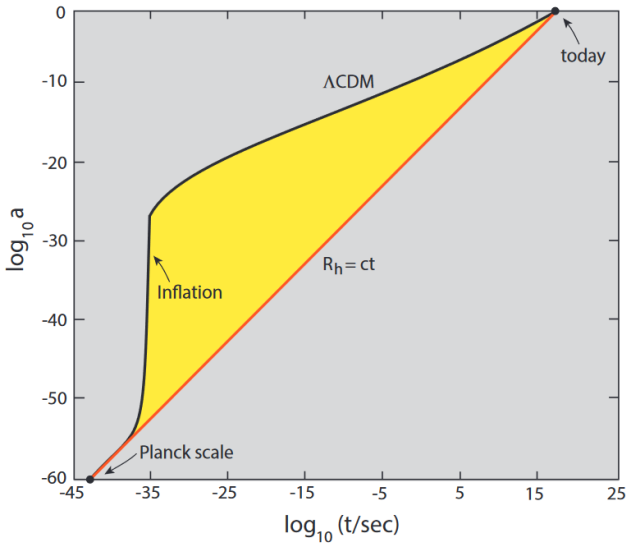

FIG. 1. The evolution of the Universe's expansion within the Planck-framework is represented by the solid black curve, while the corresponding rate for the $R_h = ct$ universe is depicted by the red line. Despite the fact that the $R_h = ct$ model avoids horizon issues and eliminates the need for the speculative inflationary paradigm, the standard cosmological model struggles to adequately explain the current state of the Universe without invoking a rapid de Sitter-like expansion phase at approximately $t \sim 10^{-37}$s. Despite experiencing various periods of deceleration and acceleration, the net expansion of the ΛCDM universe throughout a Hubble time ultimately mirrors what it would have been after a more than 60 magnitudes of continuous expansion in $R_h = ct$. That this equality occurs precisely at the present moment, when we are observing it, is an exceedingly improbable event, representing one of the most significant coincidences in conventional cosmology. Ref to fig 1 in [12].

II. MAIN PROPERTIES

A. The FRW Equations

The foundation of standard cosmology lies in the FRW metric, which describes a spatially homogeneous and isotropic three-dimensional space, wherein the coordinates either expand or contract depending on the time variable:

$$\mathrm{d}s^2 = c^2\ \mathrm{d}t^2 - a^2(t)\left[\mathrm{d}r^2\left(1-kr^2\right)^{-1} + r^2\left(\ \mathrm{d}\theta^2 + \sin^2\theta\ \mathrm{d}\phi^2\right)\right] \tag{3}$$

In this metric, the coordinates are selected such that t denotes the time perceived by a comoving observer, maintaining uniformity across the system as a 'community' time. The symbol $a(t)$ signifies the expansion factor, while r is the scaled radial coordinate suited for the comoving frame. The geometric constant k is defined as $+1$ for a closed universe, 0 for a flat universe, and 1 for an open universe.

Utilizing the FRW metric in conjunction with Einstein's field equation results in the derivation of the Friedmann equation,

$$H^2 \equiv \left(\frac{\dot{a}}{a}\right)^2 = \frac{8\pi G}{3c^2}\rho - \frac{kc^2}{a^2}, \tag{4}$$

and the "acceleration" equation,

$$\frac{\ddot{a}}{a} = -\frac{4\pi G}{3c^2}(\rho + 3p). \tag{5}$$

The overdot symbol signifies a derivative with respect to cosmic time t, while ρ and p denote the total energy and total pressure, respectively. By further employing the FRW metric in conjunction with the energy conservation equation in general relativity, the resulting final equation can be derived.

$$\dot{\rho} = -3H(\rho + p), \tag{6}$$

which is dependent with Equation 4 and 5.

B. The Birkhoff Theorem and its Corollary

According to the Birkhoff Theorem, within a spacetime exhibiting spherical symmetry, the sole solution to the Einstein equations under vacuum conditions is the

Schwarzschild exterior solution. Additionally, any vacuum solution with spherical symmetry in the exterior region must inherently be static. Birkhoff aimed to demonstrate that, analogous to Newtonian theory, the external gravitational field of a spherically symmetric matter distribution in General Relativity remains unaffected by radial pulsations occurring internally.

The aforementioned result extends a classic conclusion from Newtonian physics, which is similarly applicable in electrodynamics, stating that the gravitational influence within a spherical shell is nullified. According to Birkhoff's theorem, the implication is that the metric within a void spherical cavity, positioned at the center of a spherically symmetric framework, should match the flat-space Minkowski metric. Space will be flat within a spherical cavity irrespective of the infinity of the system. The nature of the materials surrounding the cavity is irrelevant, provided the medium maintains spherical symmetry.

Assuming a spherically symmetric mass is positioned at the center of the cavity, Birkhoff's theorem and its corollary stipulate that the metric spanning the region between this mass and the cavity's boundary inherently assumes the Schwarzschild form

$$\begin{aligned} \mathrm{d}s^2 =& c^2\ \mathrm{d}T^2\left[1-2GM/c^2R\right]-\mathrm{d}R^2\left[1-2GM/c^2R\right]^{-1} \\ &-R^2\left(\ \mathrm{d}\theta^2+\sin^2\theta\ \mathrm{d}\phi^2\right). \end{aligned} \tag{7}$$

This is the Schwarzschild's (vacuum) solution describing the spacetime around an enclosed, spherically symmetric object of mass M. Consequently, worldlines associated with an observer within this area experience curvature relative to the cavity's center, dictated exclusively by the mass situated at the center. This scenario may seemingly conflict with our isotropy assumption, which might be simplistically interpreted as suggesting that the spacetime curvature within the medium should negate itself, given that the observer perceives mass energy uniformly distributed in every direction. However, the worldlines of the observer are indeed curved in all directions, as stated by the corollary to Birkhoff's theorem; it indicates that only the mass energy located between any two specific points in this medium influences the trajectory connecting those points.

Thus, the space-time curvature along a worldline connecting any point in the universe to an observer located at a distance R can be ascertained by evaluating the mass-energy contained within a sphere of radius R centered at the origin, which is the observer's position. The mass-energy existing beyond this volume exerts no net influence on observations conducted within the sphere. Building upon this idea, a novel coordinate system is required to directly derive this effect from the transformed metric as presented in Equation 3. It has been demonstrated that our observational boundary distinctly aligns with the distance beyond which the curvature of spacetime obstructs any signal from reaching us.

C. General Coordinate Transformation

For educational clarity, it could be beneficial at this juncture to draw an analogy between our two coordinate systems and those typically employed in the context of a gravitationally collapsed entity. The comoving coordinates—or cosmic time—serve roles akin to those of an observer in freefall under the object's gravitational influence, while our new coordinates align with those of an accelerated frame, similar to an observer stationed at a static spatial point within the surrounding spacetime. A key distinction lies in the fact that the newly introduced coordinates (cT, R, θ, ϕ) are reliant on the observer, and therefore are not universally applicable nor necessarily required to be. In the framework of comoving coordinates, the proper distance $R(t)$ is determined while keeping time t fixed. As indicated by Equation 3, for radial paths in a flat cosmological model, we have $R(t) = a(t)r$. It is occasionally advantageous to re-express Equation 3 in terms of $R(t)$, as this may demonstrate how the metric coefficients are influenced by the observer's gravitational horizon, a concept that we will subsequently define.

It is convenient to define the $a(t)$ in Equation 3 using a new function $f(t)$ ref from [6]

$$a(t) = e^{f(t)} \tag{8}$$

In that case,

$$ds^2 = c^2dt^2 - e^{2f(t)}\left[dr^2 + r^2d\Omega^2\right], \tag{9}$$

where

$$d\Omega^2 \equiv d\theta^2 + \sin^2\theta d\phi^2. \tag{10}$$

So

$$r = Re^{-f}, \tag{11}$$

and therefore

$$dr = e^{-f}[dR - R\dot{f}dt], \tag{12}$$

so that

$$dr^2 = e^{-2f}\left[dR^2 + \left(\frac{R\dot{f}}{c}\right)^2 c^2dt^2 - 2\left(\frac{R\dot{f}}{c}\right)cdtdR\right]. \tag{13}$$

Collecting terms ans completing the square, we can now write the metirc as

$$ds^2 = \Phi\left[cdt + \left(\frac{R}{R_\mathrm{h}}\right)\Phi^{-1}dR\right]^2 - \Phi^{-1}dR^2 - R^2d\Omega^2. \tag{14}$$

Where, we define the quantities

$$\Phi \equiv 1 - \left(\frac{R}{R_\mathrm{h}}\right)^2, R_\mathrm{h} \equiv c/\dot{f}, \tag{15}$$

The R_h is the radiu of the cosmic horizon for the observer at the origin .

D. The Cosmic Horizon

In comparison to the Schwarzschild factor $[1 - 2GM/c^2R]$ in Equation 7, this transitions to $[1 - (R/R_{\rm h})^2]$ in eqaution 14. At a specified interval s, the observer-dependent time T markedly diverges as R approaches $R_{\rm h}$. This represents the critical distance at which the spacetime curvature precludes any signal from reaching us; the parameter R_0 is the sole (classical) scale within the system. Therefore, it is logically consistent, given the corollary to Birkhoff's theorem, that this parameter is characterized as a Schwarzschild radius or gravitational radius:

$$R_{\rm h} = \frac{2GM(R_{\rm h})}{c^2}, \tag{16}$$

$R_{\rm h}$ is the distance at which the enclosed mass is sufficient to turn it into the Schwarzschild radius for an observer at the origin of the coordinates. Where, $M(R_{\rm h})$ defined as

$$M(R_{\rm h}) = V_{\rm prop}\frac{\rho(t)}{c^2} = \frac{4\pi}{3}R_{\rm h}^3\frac{\rho(t)}{c^2}. \tag{17}$$

The FRW equations theoretically permit a multitude of solutions, each characterized by its unique form of the expansion factor $a(t)$. However, upon applying the constraint detailed in Equation 16, it becomes evident that only a singular solution is permissible as dictated by Equation 4:

$$\begin{aligned} H^2 =& \frac{8\pi G}{3c^2}\rho - \frac{kc^2}{a^2} \\ =& \frac{8\pi G}{3c^2}\frac{3c^4}{8\pi G R_{\rm h}^2} - \frac{kc^2}{a^2} \\ =& \frac{c^2}{R_{\rm h}^2}, \end{aligned} \tag{18}$$

where we have here assumed a flat universe with $k = 0$, as indicated by the precision measurements of the CMB radiation [13]. Thus we have

$$R_{\rm h} = ct. \tag{19}$$

For all cosmic times t, not just the current value t_0. In this situation, from Equation 5, we infer that the acceleration $\ddot{a} = 0$ either for an empty universe (in which $= p = 0$) or one characterized by an equation of state $\omega = -1/3$.

In this situation, the necessity of inflation to address the horizon problem, which is prevalent in the ΛCDM model, is effectively eliminated. The horizon problem arises from the observed uniformity of the Cosmic Microwave Background (CMB), where regions on opposite sides of the sky seem to have been causally disconnected due to the finite speed of light. The standard ΛCDM model requires inflation to explain how these regions could have come into thermal equilibrium[11]. However, the $R_h = ct$ model, as demonstrated by Melia [10], does not have this issue.

In the $R_h = ct$ framework, the universe expands in such a way that regions that would otherwise be outside each other's causal horizon remain connected throughout the expansion process. This eliminates the need for an inflationary period that was originally proposed to solve this problem. In contrast to ΛCDM, where inflation is a key component to reconcile the observed uniformity of the universe, the $R_h = ct$ universe naturally accommodates the causally connected regions without requiring inflation.

For example, the analysis of photon geodesics and proper distances in the $R_h = ct$ reveals that even regions on opposite sides of the universe, which in ΛCDM would be causally disconnected, have remained in contact since the early universe[10]. This is a direct consequence of the different expansion dynamics between the two models, where the $R_h = ct$ universe does not require the rapid expansion seen in inflationary models.

III. EVIDENCES SUPPORTED

A. The luminosity distance

High-redshift objects can serve as tools for testing the ΛCDM and $R_h = ct$ cosmological models. As can be seen from [14], there exists the formula

$$\begin{aligned} D_L^{\Lambda\rm CDM} = & \frac{c}{H_0}\frac{(1+z)}{\sqrt{|\Omega_k|}}{\rm sinn}\{|\Omega_k|^{\frac{1}{2}} \times \\ & \int_0^z \frac{1}{\sqrt{\Omega_m(1+z)^3 + \Omega_k(1+z)^2 + \Omega_{de}(1+z)^{3(1+\omega_{de})}}}\,dz\} \end{aligned} \tag{20}$$

$$D_L^{R_h=ct} = \frac{c}{H_0}(1+z)\ln(1+z) \tag{21}$$

The former represents the luminosity distance in the ΛCDM model, while the latter represents the luminosity distance in the $R_h = ct$ model. The luminosity distances in the two models will exhibit significant differences at high redshifts.

Select HII galaxies (HIIGx) and Giant Extragalactic HII Regions (GEHR) as standard candles, which can be observed at high redshifts. By observing data, the true distance modulus is obtained from

$$\mu_{obs} = 2.5[\kappa + \alpha\log\sigma(H\beta) + \log F(H\beta)] - 100.2 \tag{22}$$

and the theoretical luminosity distance is calculated using the model, from which the theoretical distance modulus is obtained through

$$\mu_{th} = 5\log[\frac{D_L(z)}{Mpc}] + 25 \tag{23}$$

The cosmological constant for different models is determined using the maximum likelihood method

$$\mathcal{L} = \prod_i \frac{1}{\sqrt{2\pi}\sigma_{\mu_{obs,i}}} \times \exp\left[-\frac{(\mu_{obs,i} - \mu_{th}(z))^2}{2\sigma^2_{\mu_{obs,i}}}\right] \quad (24)$$

The obtained data is shown in Table I.

Model	α	δ	Ω_m	Ω_{de}
$R_h = ct$	$4.86^{+0.08}_{-0.07}$	$32.38^{+0.29}_{-0.29}$	-	-
ΛCDM	$4.89^{+0.09}_{-0.09}$	$32.49^{+0.35}_{-0.35}$	$0.40^{+0.09}_{-0.09}$	$1.0 - \Omega_m$
ωCDM	$4.87^{+0.10}_{-0.09}$	$32.40^{+0.36}_{-0.36}$	$0.22^{+0.16}_{-0.14}$	$1.0 - \Omega_m$

Model	ω_{de}	$-2\ln\mathcal{L}$	AIC	KIC	BIC
$R_h = ct$	-	559.98	563.98	565.98	570.08
ΛCDM	-1 (fixed)	563.77	569.77	572.77	578.92
ωCDM	$-0.51^{+0.15}_{-0.25}$	561.12	569.12	573.12	581.32

TABLE I. Best-fitting results in different cosmological models. Ref to Table 2 in [14].

Several model selection tools commonly used to differentiate between cosmological models [15]include the Akaike Information Criterion,AIC $= -2\ln\mathcal{L}+2n$,wheren is the number of free parameters[16–19],the Kullback Information Criterion,KIC $= -2\ln\mathcal{L} + 3n$[20],and the Bayes Information Criterion,BIC $= -2\ln\mathcal{L} + (\ln N)n$,where N is the number of data points[21]. In the case of AIC, with AIC_α characterizing model M_α, the unnormalized confidence that this model is true is the Akaike weight $\exp(-\mathrm{AIC}_\alpha/2)$. Model M_α has likelihood

$$P(\mathrm{M}_\alpha) = \frac{\exp(-\mathrm{AIC}_\alpha/2)}{\exp(-\mathrm{AIC}_1/2) + \exp(-\mathrm{AIC}_2/2)} \quad (25)$$

of being the correct choice in this one-on-one comparison.

All three statistical methods indicate that $R_h = ct$ is preferred over both the ΛCDM and ωCDM models, with the likelihood for the former exceeding 90% in all cases

B. JWST Observations

Over the past two years, the collected high-precision data from three different sources, as we will state in this section below, these findings consistently indicate that the timeline predicted by the standard ΛCDM model is significantly contradicted by the observations.

The early emergence of (i) well-formed galaxies[22] and (ii) $10^9 M_\odot$ supermassive black holes[23] has been widely discussed. Evidence from high-redshift galaxies ($z \sim 16$) and quasars ($z \sim 10$) strongly supports the timeline in the $R_h = ct$ universe, whereas the latest findings reported by *JWST* further challenge the timeline within the ΛCDM framework. Conversely, (iii) Witstok et al.[24] identified compelling evidence of the ultraviolet attenuation 'bump,' associated with PAHs, i.e., nano-sized graphitic grains[25], in the spectrum of a galaxy at $z = 6.71$. Basic astrophysical principles would require a much longer time for these carbonaceous dust grains to form than the age of the ΛCDM universe at that redshift (see figure 2 left). In contrast, all three of these categories of source self-consistently follow the timeline predicted by the $R_h = ct$ universe (figure 2 right).

1. *Early Galaxies*

JWST has identified a large population of high-z galaxies, including candidates at $z \sim 16 - 17$, within a short period after its deployment [26–28]. Spectroscopic confirmations have verified photometric redshifts up to at least $z \sim 13$ [29]. However, these findings challenge the expected timeline of galaxy formation in ΛCDM.

Based on Planck-optimized parameters ($H_0 = 67.4 \pm 0.5$ km s^{-1} Mpc^{-1}, $\Omega_m = 0.315 \pm 0.007$), ΛCDM predicts that significant galaxy formation should not have commenced until several hundred Myr after the Big Bang [30]. The detection of well-formed stellar structures with masses of $\sim 10^9 M_\odot$ at $z \sim 16 - 17$ implies that these galaxies must have assembled within ~ 230 Myr after the Big Bang [22]. However, numerical simulations indicate that the condensation of baryonic gas and formation of Population III (Pop III) stars within dark matter halos of $M_{\rm halo} \sim 10^6 M_\odot$ could not have occurred significantly earlier than $z \sim 20$, as radiative cooling and feedback processes would have imposed substantial delays [31, 32].

The major inconsistency lies in the rapid formation of massive galaxies within $\sim 70 - 90$ Myr, which no simulation has yet been able to replicate [33]. Even introducing increased scatter in cooling times and weaker Pop III supernovae [34, 35] does not sufficiently alleviate the tension. If the inferred growth rate of galaxies such as S5-z17-1 is modeled as [33]:

$$\frac{dM}{dt} = K \exp\left(\frac{t - t^*}{t_c}\right), \quad (26)$$

where t_c is the characteristic timescale for star formation, then the results imply an implausibly early onset of star formation ($z \sim 28$) in ΛCDM [22]. In contrast, the $R_h = ct$ cosmology offers a more extended timeline, allowing ample time for these galaxies to form within an astrophysically reasonable framework [22].

2. *The Challenge of Early Supermassive Black Holes*

The discovery of the supermassive black hole (SMBH) UHZ-1 at $z = 10.073$ [36] exacerbates the timeline inconsistency in ΛCDM. The standard model predicts that black hole growth is constrained by Eddington-limited accretion, described by:

$$\frac{dM}{dt} = \frac{1.3 \times 10^{38}\mathrm{erg/s}}{\epsilon c^2 M_\odot} M. \quad (27)$$

For a seed black hole of $M_{\rm seed} \sim 10M_\odot$, the Salpeter timescale suggests that reaching $M \sim 10^8 M_\odot$ would require at least ~ 600 Myr, yet ΛCDM allows only ~ 300 Myr before $z = 10$, making standard growth mechanisms insufficient.

Proposed solutions include super-Eddington accretion and direct collapse black hole (DCBH) formation, but observational evidence remains lacking. For example, no known high-z quasar has been confirmed to be accreting significantly above the Eddington limit [37]. Additionally, while the DCBH scenario proposes massive $10^5 M_\odot$ seeds, no direct evidence of such an early formation channel has been identified.

In contrast, the $R_h = ct$ model provides a longer cosmic timeline, wherein UHZ-1 would have emerged at $z \sim 20$, allowing ~ 600 Myr for its growth—a scenario that aligns with current astrophysical models of Pop III star evolution and SMBH seeding mechanisms [22].

3. *Unexpected PAH Detection in the Early Universe*

JWST observations of the galaxy JADES-GS-z6-0 at $z = 6.71$ (~ 900 Myr in ΛCDM) revealed strong evidence for an absorption feature at $\lambda_{\rm emit} = 2175$ Å, attributed to polycyclic aromatic hydrocarbons (PAHs) [24]. PAHs are expected to form primarily through asymptotic giant branch (AGB) stars, which require at least ~ 1 Gyr to evolve [38], creating a significant time compression problem.

Conventional ΛCDM models predict that at $z = 6.71$, the first stars were only ~ 500 Myr old, making it unlikely for AGB stars to have contributed significant dust production. While alternative scenarios such as PAH formation in massive Wolf-Rayet (WR) stars or supernova ejecta have been proposed [39], these mechanisms are highly speculative, as WR stars are rare and supernovae typically destroy more dust than they create [40].

In contrast, in the $R_h = ct$ model, the detection of PAHs at $z = 6.71$ corresponds to ~ 1.7 Gyr after the Big Bang, providing sufficient time for AGB stars to produce the required dust. This alleviates the time compression issue seen in ΛCDM, offering a more consistent timeline for the emergence of early dust [22].

C. ω_{de}-Ω_m constraint

Over the past decade, ω_{de} and Ω_m have been measured with high precision. But we can only gain the value range of these two parameters, not their unique values. The reason for this is that, other than the Sachs-Wolfe effect, which is responsible for the largest angular fluctuations in the CMB, none of the other mechanisms producing structure of one kind or another depends sensitively on the expansion history of the Universe. As such, some degeneracy exists among the possible choices of cosmological parameters pertaining to the CMB.[41]

Nonetheless, all of the constraints derived from the observations produce a similar region in ω_{de}-Ω_m phase space The confidence regions shown in Figure 3 are adapted from a corresponding figure in Melchiorri et al. (2003)[44]. These show the 68%, 95%, and 99% confidence regions corresponding to the Type Ia SNe observations (adapted from Suzuki et al. 2012, shown as gray swaths), and the corresponding regions inferred from the analysis of CMB, HST, and 2dF data (indicated by the lighter colored island regions to the upper left of this diagram).[41]

The most important part of Figure 3 is the thick black curve. Now we derive this curve. We assume that $k = 0$ as in Equation 18. This also means that $\Omega \equiv \Omega_r + \Omega_m + \Omega_{de} = 1$. Then, we integrate the Equation 18, and we have

$$ct_0 = R_h(t_0) \int_0^1 \frac{udu}{\sqrt{\Omega_r + \Omega_m u + \Omega_{de} u^{1-3\omega_{de}}}} \tag{28}$$

To obtain Equation 28, we have allowed the possibility that dark energy is not a cosmological constant (i.e., that ω_{de} may be not 1, in which case we would refer to this model as wCDM, rather than ΛCDM), and we have used the derived value of the gravitational horizon to write $R_h = \frac{c}{H}$ (Melia 2007[5]; Melia Shevchuk 2012[7]). This equation also assumes that $a \to 0$ at $t = 0$.

As we have obtained the Equation 19, Equation 28 can be written as

$$I = \int_0^1 \frac{udu}{\sqrt{\Omega_r + \Omega_m u + \Omega_{de} u^{1-3\omega_{de}}}} \tag{29}$$

for any given ω_{de}, there is only one value of Ω_m that satisfy the equation. This is the expression of the curve in the Figure 3. It illustrates what values of ω_{de} and Ω_m are permitted in the $R_h = ct$ universe.

ΛCDM can't explain why the most possible region of the allowed values is limited as in the Figure 3 and why these two observations have the overlapping area in the figure. But for the $R_h = ct$ universe, it is the region that allowed by the Equation 29. What's more, the WMAP measurements (Bennett et al. 2013[42]), which is the black dot, and the Planck measurements (Ade et al. 2013[43]), which is the black star just located beside the curve closely. The theory of $R_h = ct$ universe gives a good prediction.

IV. ARGUMENTS

A. The influence of matter

1. *The cosmic evolution curve*

Consider a universe with two energy density components: matter with a zero equation of state and dark energy with an equation of state parameter ω, while neglecting the impact of photon energy density. According

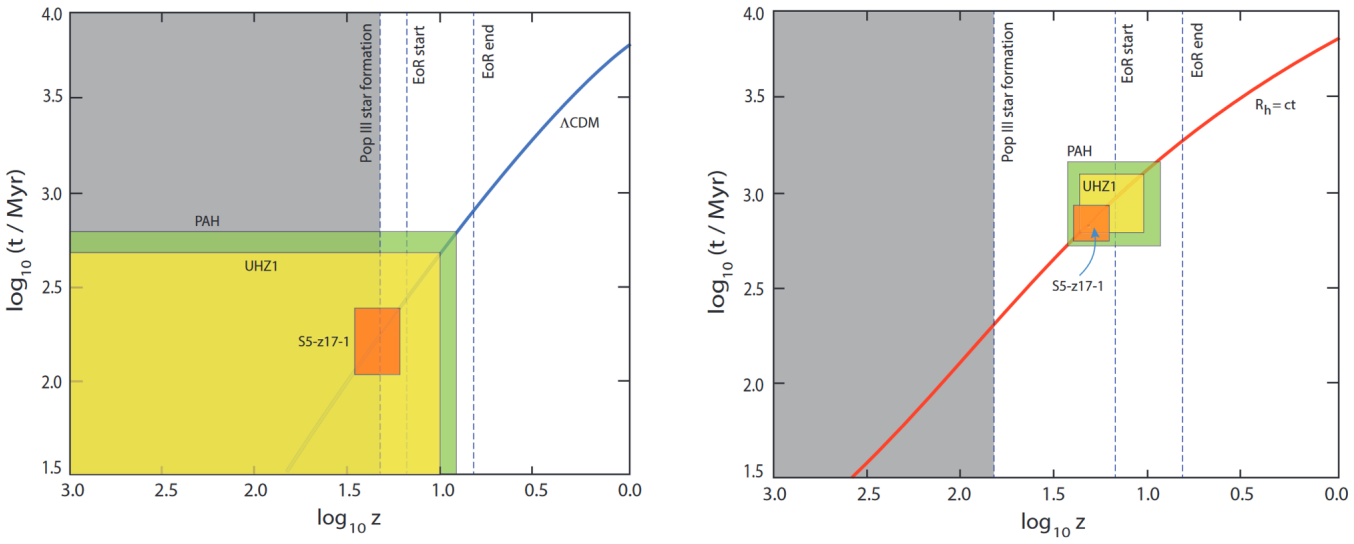

FIG. 2. **Left:** age-redshift relation in the Planck-ΛCDM framework (solid blue curve). In this model, the "dark ages" end following the formation of Population III stars at $z \sim 20$ ($t \sim 200$ Myr). Observations suggest the Epoch of Reionization (EoR) began at $z \sim 15$ ($t \sim 280$ Myr) and ended at $z \sim 6$ ($t \sim 1$ Gyr). Under conventional astrophysical assumptions, the earliest quasar (UHZ-1) would require a formation onset before the Big Bang ($t < 0$), and the first galaxies (e.g. S5-z17-1) would need foundational processes preceding star formation. Moreover, PAHs detected at $z = 6.71$ ($t \sim 900$ Myr) are expected to take approximately 1 Gyr to form, implying an onset before the Big Bang and well before Population III stars. **Right:** Same as left, but for the $R_{\rm h} = ct$ model (solid red curve). Here, the "dark ages" end at $z \sim 50$ ($t \sim 250$ Myr), the EoR begins at $t \sim 820$ Myr ($z \sim 15$) and ends at $t \sim 1.9$ Gyr ($z \sim 6$). PAHs appear at ~ 1.7 Gyr ($z = 6.71$), forming since $z \sim 17$ ($t \sim 730$ Myr). UHZ-1 was seeded at $z \sim 20$ ($t \sim 620$ Myr) and is observed at $t \sim 1.2$ Gyr ($z = 10.1$); the galaxy S5-z17-1 began its growth at $t \sim 500$ Myr ($z \sim 25$) and is observed at ~ 750 Myr ($z \sim 16$). Ref to figure 2 and figure 3 in [12].

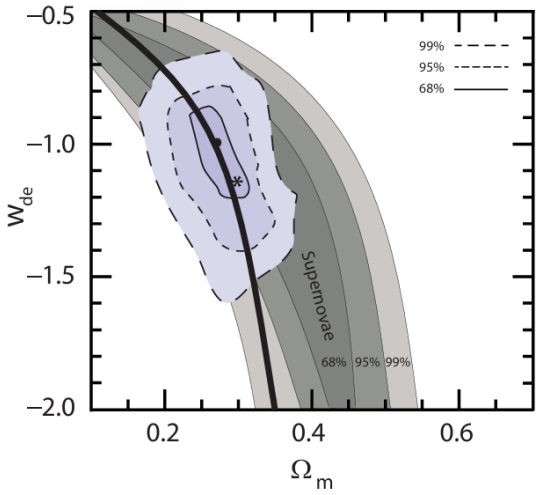

FIG. 3. The solid black curve indicates the value ω_{de} and Ω_m must have in the R_h = ct universe. The location (black dot) of the WMAP measurements (Bennett et al.2013[42]), versus (star) the latest measurements by Planck (Ade et al. 2013 [43]), which resulted in the values $\Omega_m \approx 0.3$ and $\omega_{de} \approx -1.13$. The value $\Omega_m = 0.27$ is realized only when $\omega_{de} = -1$

.

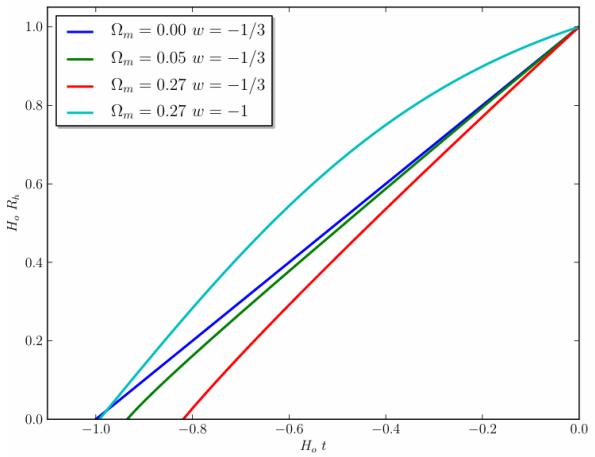

FIG. 4. The cosmic horizon, R_h, as a function of cosmic time for various cosmological models. The dark blue line represents massless universe, containing only a dark energy component with $\omega = -\frac{1}{3}$, while the green and red lines represent similar cosmological models but with present-day normalized mass densities of 0.05 and 0.27, respectively. The cyan line corresponds to a ΛCDM universe with $\omega = -1$. Ref to figure 1 in [45]

to [45], the cosmic evolution under different matter densities can be obtained from

$$H \equiv \frac{\dot{a}}{a} = H_0\sqrt{\Omega_m a^{-3} + \Omega_{de} a^{-3(1+\omega)}} \tag{30}$$

as shown in Figure 4, Figure 5

In Figure 4,the blue curve represents the $R_h = ct$ model with a matter density of 0, where the evolution of

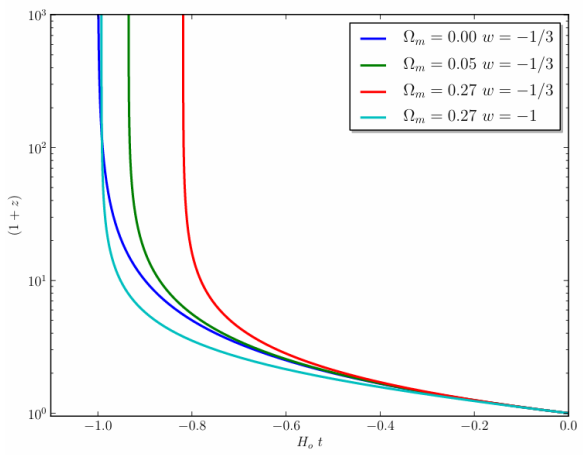

FIG. 5. As Figure 4, but presenting the redshift, as observed today, as a function of cosmic time. Ref to figure 2 in [45].

the cosmic horizon is linear. The green curve introduces a slight amount of matter with a density of 0.05, showing that the evolution of the cosmic horizon is still approximately linear. Although it aligns with the $R_h = ct$ model in the present, it diverges significantly from the $R_h = ct$ evolution curve in the early universe. The red curve, which includes the current matter density of 0.27, shows an even greater deviation. The cyan curve represents the ΛCDM model, with a current matter density of 0.27.

In Figure 5, it can also be observed that as the matter content increases, the evolution curve of the cosmic horizon increasingly deviates from the $R_h = ct$ evolution pattern.

From the observation of Figure 4, one can immediately draw the conclusion: if the equation of state for the dark energy component of the universe satisfies $\omega = -\frac{1}{3}$, then the presence of any matter will cause the universe to deviate from the strictly required $R_h = ct$ cosmological evolution.

2. *Look-back time verses redshift*

The advantage of the $R_h = ct$ model is that it addresses the problem of high-redshift quasars and the growth of supermassive black holes within a finite time after the Big Bang, which the ΛCDM model cannot[46].

If we assume that supermassive black holes did not exist originally but instead grew from black holes formed by the first generation of stars, then there exists a relationship [46]

$$M = M_0 \exp\left(\frac{\tau_{M_0}}{45\text{Myrs}}\right) \tag{31}$$

Therefore, based on black hole mass estimates and observation time, we can retroactively infer the time of formation of the black hole seed. A set of data from Table in [46] is used as a sample. As shown in Figure 6, the

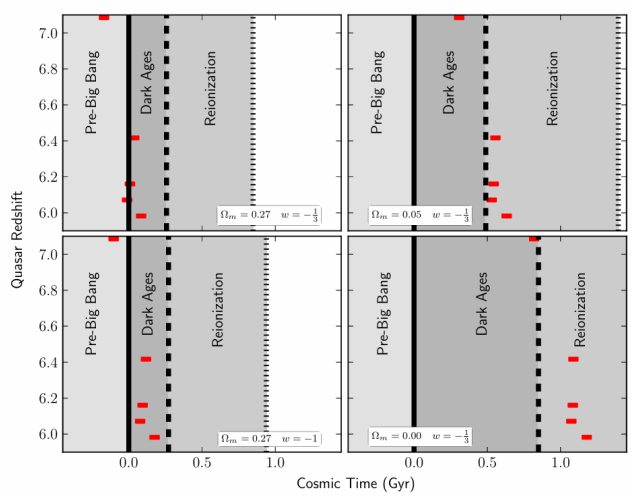

FIG. 6. The figure uses $5M_\odot$ and $20M_\odot$ seed black holes.The Big Bang is represented by a vertical solid black line, while the end of the Dark Ages is marked by a dashed line. A red horizontal bar indicates the period of seed black hole formation as described. The bottom left panel illustrates the case of $\Omega_m = 0.27$ and $\omega = -1$, corresponding to the ΛCDM cosmological model, while the bottom right panel shows the scenario with $\Omega_m = 0.00$ and $\omega = -\frac{1}{3}$, corresponding to the $R_h = ct$ cosmological model. The top panels display cosmological models incorporating a dark energy component $\omega = -\frac{1}{3}$ but with different matter density parameters: the top left panel features $\Omega_m = 0.27$, and the top right panel features $\Omega_m = 0.05$. Ref to figure 3 in [45].

red band corresponds to the period during which seed black holes with masses between 20M and 5M must have formed in order to produce the quasars we observe today (this is equivalent to Figure 1 in [46]).

In the ΛCDM model, seed black holes need to form during the "dark ages," which occurs before supernova explosions. In the $R_h = ct$ model, the seed formation time for quasars occurs at a later stage of the universe, most of which happens after the "dark ages," during the reionization era, when massive stars can easily form seed black holes. However, the presence of matter reduces this advantage. At a matter density of 0.05, the formation period is delayed to just after the dark ages. At a more realistic matter density of 0.27, the formation period of black hole seeds is now pushed back into the depths of the "dark ages," and some seed black holes may even need to have formed during or before the "big bang" period.

The presence of matter significantly weakens the claimed advantage of the $R_h = ct$ model in providing sufficient time for the formation of supermassive black holes in the early universe.

3. *Evolving dark energy?*

If dark energy can deviate, does the $R_h = ct$ model still have a chance? If ω is less than 0, the universe becomes

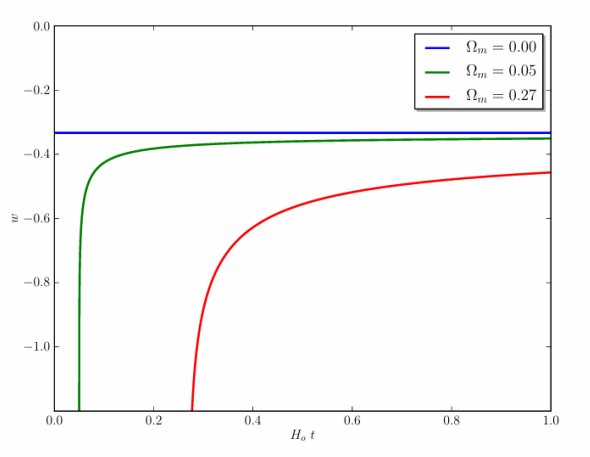

FIG. 7. The evolving equation of state,ω, as a function of cosmic time, required to ensure that $R_h = ct$. With the presence of any non-zero matter component, ω becomes unphysical at suficiently early times. Ref to figure 5 in [45].

matter-dominated in the early universe. If ω is greater than 0, the universe becomes energy-dominated in the early universe, which increases the degree of deviation in the evolution curve of the cosmic horizon. Therefore, an attempt is made to find a time-varying ω to achieve the required expansion.

For the $R_h = ct$ model, there exists

$$a\sqrt{\Omega_m a^{-3} + \Omega_{de} a^{-3(1+\omega)}} = 1 \tag{32}$$

which can be rearranged to express ω as a function of cosmic time t.

$$\omega = -\frac{1}{3}(1 + \log \frac{1 - \Omega_m/(H_0 t)}{\Omega_{de}} / \log H_0 t) \tag{33}$$

it is required that

$$H_0 t \geq \Omega_m \tag{34}$$

Figure 7 presents this evolution for several ducial cosmologies. As expected, with no matter content ($\Omega_m = 0$), the equation of state of the dark energy is constant at $\omega = -\frac{1}{3}$. However, in the other two cases, with $\Omega_m = 0.05$ (green line) and $\Omega_m = 0.27$ (red line), then ω significantly deviates from this value. And both models cross the 'Phantom Divide' ($\omega = -1$), before diverging to $\omega = -\infty$

Hence,considering Equation 34, for any universe with matter, there is no equation of state for dark energy that ensures the existence of $R_h = ct$.

B. The evidence of accelerated expansion

We start from null hypothesis, one is called no acceleration, which is Equation 35; another is called no superacceleration, which is Equation 36.

$$q(t) \equiv -\frac{\ddot{a}}{aH^2} \geq 0 \tag{35}$$

$$\dot{H} - \frac{k}{a^2} \leq 0 \tag{36}$$

Rh=ct universe is when $q = 0$. The universe expands at a constant rate all the time[37].

For the convenience of using the null hypothesis, we derive two new equations from the null hypothesis[37].

The deceleration parameter $q(t)$ can be related with the Hubble parameter $H(t)$ as

$$\ln \frac{H(z)}{H_0} = \int_0^z \frac{1 + q(z')}{1 + z'} dz' \tag{37}$$

Substituting Equation 35 into Equation 37, we have

$$H(z) \geq H_0(1 + z) \tag{38}$$

Hubble constant H_0 denotes the current value of the Hubble parameter $H(z)$.

for Equation 36. Integrating directly, we have

$$H(z) \geq H_0 \sqrt{1 - \Omega_k + \Omega_k(1 + z)^2} \tag{39}$$

where $\Omega_k = -\frac{k}{a_0 H_0^2}$. For a spatially flat universe, $\Omega_k = 0$, the above equation becomes

$$H(z) \geq H_0 \tag{40}$$

Now we have the following new No Acceleration condition (Equation 41) and No Super-acceleration condition (Equation 42)

$$E(z) \geq (1 + z) \tag{41}$$

$$E(z) \geq 1 \tag{42}$$

where $E(z) = \frac{H(z)}{H_0}$.

If the universe has never experienced an accelerated expansion or the expansion is always decelerating, then Equation 41 is always satisfied. Therefore, this equation can be used to obtain direct model-independent evidence for cosmic acceleration.

However, we must be cautious to interpret the result correctly. Because of the integration effect, even if the Equation 41 is satisfied at some redshifts, it does not mean that the universe has never experienced an accelerating expansion[47],[48]. If the Equation 41 is violated at some redshifts, we are sure that the universe once experienced accelerating expansion. Now we use the Pantheon+MCT Sne Ia measurements on $E(z)$ to show the evidence of cosmic acceleration expansion. The advantage of the $E(z)$ data[49] is that it is independent of the Hubble constant and the drawback is that it assume $k = 0$, so it is model dependent in this sense.

We plot the measurements $E(z)$ data at six redshifts with 1σ, 2σ, 3σ errors and $1 + z$, 1 on the Figure 8. We can see that all the low redshift data points are at out of the deceleration region even at 3σ level. As a result, the universe has experienced accelerated expansion. The Pantheon+MCT Sne Ia data is strongly against the $R_h = ct$ universe.

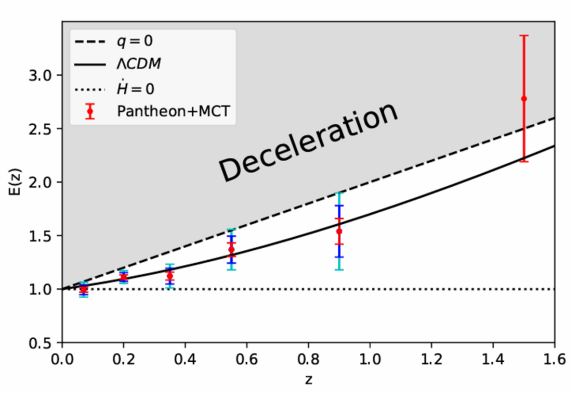

FIG. 8. The Pantheon+MCT SNe Ia measurements on $E(z)$ with 1σ, 2σ, 3σ errors. The dashed line corresponds to the $R_h = ct$ model with $q(z) = 0$, the dotted line denotes $E(z) = 1$ which represents the model with $\dot{H} = 0$ in a spatially at universe, and the solid line shows the best fit ΛCDM model.[37]

V. SUMMARY AND DISCUSSION

In this review, we started with the coincidence that now the deceleration of the Hubble–Lemaitre flow is compensated by the acceleration of the dark energy; the average acceleration throughout the history of the universe is almost null and the size of the universe is such as if there were constant expansion[5], and introduce the derivation and main properties of $R_h = ct$ universe supported by this coincidence. Due to the evidence backing it, this hypothesis provides additional advantages at high z. In this context, the standard model struggles to account for the presence of objects that typically require extensive time to form, in the youthful universe that does not permit sufficient time for such evolution. $R_h = ct$ solves the problem because the age of the universe at redshift $z, t(z)$, is much greater in this model than with the standard ΛCDM. The Big Bang would have happened $H_0^{-1} = 14.57$ Gyr ago (for $H_0 = 67.4$ km/s/Mpc), longer than the 13.79 Gyr for ΛCDM with the same Hubble constant[12]. There would have been no inflation.

Nevertheless, theoretical derivation presents certain uncertainties [50], particularly regarding the applicability of the Schwarzschild radius on such extensive scales. A fundamental presumption in deriving the Schwarzschild radius is that the space-time is static. This assumption may not hold when considering expanding regions. Additionally, it is important to highlight that a particular spacetime geometry can be represented through various coordinate systems, and not every characteristic of the metric inherently holds physical significance. A notable illustration of this is the divergence observed at the event horizon in the Schwarzschild metric, which, when expressed in Eddington-Finkelstein coordinates, can be demonstrated to be a coordinate singularity.[51]. A notably distinct aspect of this model when compared to the

standard model is its assertion that the CMB originates at $z \approx 16$ through the rethermalization of Population III starlight by dust [52]. However, a significant challenge lies in explaining how a perfect blackbody spectrum could arise, given that no known type of dust generates such a spectral form. This alternative explanation of the CMB significantly diverges from the standard model. Moreover, achieving a state in which the Universe's contents are fine-tuned to consistently result in an overall effective EOS of 1/3 is exceedingly challenging.In this case, the parameter $\omega = -1/3$ may not represent a constant value, but rather reflects the average characteristic of our universe, denoted as $< \omega >= -1/3$. An additional issue concerns the fact that the amplification of fluctuations within the $Ht = 1$ model is influenced by a negative pressure term, which appears consistent regardless of the scale of perturbation. Consequently, the manner in which large-scale structures manifest within this framework remains somewhat ambiguous.

In the observed evidences against the $R_h = ct$ universe, the presence of matter is demonstrated to compromise the strict expansion characteristics fundamental to the evolution of $R_h = ct$ cosmologies as presented. Evaluating whether a dynamic dark energy component can reconcile this type of cosmological expansion with matter by achieving an expansion aligned with an average value of $< \omega >= -1/3$, it is observed that including mass necessitates non-physical characteristics of the dark energy component in the early universe. This suggests that matter in the universe imposes substantial constraints on the essential attributes of $R_h = ct$ cosmology, indicating that an unconventional and unphysical evolution of the matter component would be necessary to preserve its viability. Apart from that, the evidence of cosmic acceleration strongly against the $R_h = ct$ universe. Despite certain predictions and implications of ΛCDM being so perplexing that alternative mechanisms have been developed to replicate the observed characteristics of accelerated expansion, substantial observational evidence, as previously mentioned, supports the presence of a cosmological constant.

Thus, although it may appear surprising that the average deceleration parameter is approximately zero at this specific moment in cosmic time, indicating that certain elements of the standard model might be artificially constructed, such arguments cannot take precedence over the constraints derived from observational data. The close equivalence between the Hubble radius R_h and the universe's age t_0 necessitates a careful interpretation and does not automatically rule out a cosmological model featuring a non-zero cosmological constant.

To conclude, while the model $R_h = ct$ offers an intriguing alternative to the standard cosmological framework, it faces substantial challenges. In contrast, the ΛCDM model, despite its own unresolved issues, continues to align well with current observational data and remains the dominant framework. Further observational data, especially from large surveys and high-redshift probes, will be crucial in testing the viability of the $R_h = ct$ model and determining whether it can provide an adequate explanation for the universe's observed acceleration, cosmic structures, and the cosmic microwave background.

[1] S. Weinberg, Gravitation and cosmology: principles and applications of the general theory of relativity, (1972).

[2] J. P. Ostriker and P. J. Steinhardt, The observational case for a low-density universe with a non-zero cosmological constant, Nature **377**, 600 (1995).

[3] L. Verde, N. Schöneberg, and H. Gil-Marín, A tale of many h 0, Annual Review of Astronomy and Astrophysics **62** (2023).

[4] F. Melia, *The Edge of Infinity: Supermassive Black Holes in the Universe* (Cambridge University Press, 2003).

[5] F. Melia, The cosmic horizon, Monthly Notices of the Royal Astronomical Society **382**, 1917 (2007).

[6] F. Melia and M. Abdelqader, The cosmological spacetime, International Journal of Modern Physics D **18**, 1889 (2009).

[7] F. Melia and A. S. H. Shevchuk, The rh=ct universe: The rh= ct universe, Monthly Notices of the Royal Astronomical Society **419**, 2579–2586 (2011).

[8] F. Melia, A comparison of the rh = ct and cdm cosmologies using the cosmic distance duality relation, Monthly Notices of the Royal Astronomical Society **481**, 4855–4862 (2018).

[9] F. Melia and M. Fatuzzo, The epoch of reionization in therh = ctuniverse, Monthly Notices of the Royal Astronomical Society **456**, 3422–3431 (2016).

[10] F. Melia, The rh =ctuniverse without inflation, Astronomy amp; Astrophysics **553**, A76 (2013).

[11] A. D. Linde, A New Inflationary Universe Scenario: A Possible Solution of the Horizon, Flatness, Homogeneity, Isotropy and Primordial Monopole Problems, Phys. Lett. B **108**, 389 (1982).

[12] F. Melia, Strong observational support for the rh=ct timeline in the early universe (2024), arXiv:2407.15279 [astro-ph.CO].

[13] D. N. Spergel, L. Verde, H. V. Peiris, E. Komatsu, M. R. Nolta, C. L. Bennett, M. Halpern, G. Hinshaw, N. Jarosik, A. Kogut, M. Limon, S. S. Meyer, L. Page, G. S. Tucker, J. L. Weiland, E. Wollack, and E. L. Wright, First-year wilkinson microwave anisotropy probe (wmap) observations: Determination of cosmological parameters, The Astrophysical Journal Supplement Series **148**, 175–194 (2003).

[14] J.-J. Wei, X.-F. Wu, and F. Melia, The h ii galaxy hubble diagram strongly favours r h= ct over λcdm, Monthly Notices of the Royal Astronomical Society **463**, 1144 (2016).

[15] F. Melia and R. S. Maier, Cosmic chronometers in the r h= ct universe, Monthly Notices of the Royal Astronomical Society **432**, 2669 (2013).

[16] H. Akaike, Information theory as an extension of the maximum likelihood principle in petrov bn & csaki f.(eds.) second international symposium on information theory (pp. 267–281) (1973).

[17] A. R. Liddle, Information criteria for astrophysical model selection, Monthly Notices of the Royal Astronomical Society: Letters **377**, L74 (2007).

[18] K. B. D. Anderson, Model selection and multimodel inference: a practical information-theoretic approach springer-verlag new york, NY, USA (2002).

[19] K. P. Burnham and D. R. Anderson, Multimodel inference: understanding aic and bic in model selection, Sociological methods & research **33**, 261 (2004).

[20] J. E. Cavanaugh, Criteria for linear model selection based on kullback's symmetric divergence, Australian & New Zealand Journal of Statistics **46**, 257 (2004).

[21] G. Schwarz, Estimating the dimension of a model, The annals of statistics , 461 (1978).

[22] F. Melia, The cosmic timeline implied by the jwst high-redshift galaxies, Monthly Notices of the Royal Astronomical Society: Letters **521**, L85–L89 (2023).

[23] F. Melia, The cosmic timeline implied by the highest redshift quasars (2024), arXiv:2412.02706 [astro-ph.CO].

[24] J. Witstok, I. Shivaei, R. Smit, R. Maiolino, S. Carniani, E. Curtis-Lake, P. Ferruit, S. Arribas, A. J. Bunker, A. J. Cameron, S. Charlot, J. Chevallard, M. Curti, A. de Graaff, F. D'Eugenio, G. Giardino, T. J. Looser, T. Rawle, B. Rodríguez del Pino, C. Willott, S. Alberts, W. M. Baker, K. Boyett, E. Egami, D. J. Eisenstein, R. Endsley, K. N. Hainline, Z. Ji, B. D. Johnson, N. Kumari, J. Lyu, E. Nelson, M. Perna, M. Rieke, B. E. Robertson, L. Sandles, A. Saxena, J. Scholtz, F. Sun, S. Tacchella, C. C. Williams, and C. N. A. Willmer, Carbonaceous dust grains seen in the first billion years of cosmic time, Nature **621**, 267–270 (2023).

[25] A. Li and B. T. Draine, Infrared emission from interstellar dust. ii. the diffuse interstellar medium, The Astrophysical Journal **554**, 778–802 (2001).

[26] K. M. Pontoppidan, J. Barrientes, C. Blome, H. Braun, M. Brown, M. Carruthers, D. Coe, J. DePasquale, N. Espinoza, M. G. Marin, K. D. Gordon, A. Henry, L. Hustak, A. James, A. Jenkins, A. M. Koekemoer, S. LaMassa, D. Law, A. Lockwood, A. Moro-Martin, S. E. Mullally, A. Pagan, D. Player, C. Proffitt, C. Pulliam, L. Ramsay, S. Ravindranath, N. Reid, M. Robberto, E. Sabbi, L. Ubeda, M. Balogh, K. Flanagan, J. Gardner, H. Hasan, B. Meinke, and A. Nota, The jwst early release observations, The Astrophysical Journal Letters **936**, L14 (2022).

[27] S. L. Finkelstein, M. B. Bagley, P. Arrabal Haro, M. Dickinson, H. C. Ferguson, J. S. Kartaltepe, C. Papovich, D. Burgarella, D. D. Kocevski, M. Huertas-Company, K. G. Iyer, A. M. Koekemoer, R. L. Larson, P. G. Pérez-González, C. Rose, S. Tacchella, S. M. Wilkins, K. Chworowsky, A. Medrano, A. M. Morales, and e. a. Somerville, A long time ago in a galaxy far, far away: A candidate z 12 galaxy in early jwst ceers imaging, The Astrophysical Journal Letters **940**, L55 (2022).

[28] T. Treu, G. Roberts-Borsani, M. Bradac, G. Brammer, A. Fontana, A. Henry, C. Mason, T. Morishita, L. Pentericci, X. Wang, A. Acebron, M. Bagley, P. Bergamini, D. Belfiori, A. Bonchi, K. Boyett, K. Boutsia, A. Calabró, G. B. Caminha, M. Castellano, A. Dressler, K. Glazebrook, C. Grillo, C. Jacobs, T. Jones, P. L. Kelly, N. Leethochawalit, M. A. Malkan, D. Marchesini, S. Mascia, A. Mercurio, E. Merlin, T. Nanayakkara, M. Nonino, D. Paris, B. Poggianti, P. Rosati, P. Santini, C. Scarlata, H. V. Shipley, V. Strait, M. Trenti, C. Tubthong, E. Vanzella, B. Vulcani, and L. Yang, The glass-jwst early release science program. i. survey design and release plans, The Astrophysical Journal **935**, 110 (2022).

[29] B. E. Robertson, S. Tacchella, B. D. Johnson, K. Hainline, L. Whitler, D. J. Eisenstein, R. Endsley, M. Rieke, D. P. Stark, S. Alberts, A. Dressler, E. Egami, R. Hausen, G. Rieke, I. Shivaei, C. C. Williams, C. N. A. Willmer, S. Arribas, N. Bonaventura, A. Bunker, A. J. Cameron, S. Carniani, S. Charlot, J. Chevallard, M. Curti, and e. a. Curtis-Lake, Identification and properties of intense star-forming galaxies at redshifts zgt;10, Nature Astronomy **7**, 611–621 (2023).

[30] N. Aghanim, Y. Akrami, M. Ashdown, J. Aumont, C. Baccigalupi, M. Ballardini, A. J. Banday, R. B. Barreiro, N. Bartolo, S. Basak, R. Battye, K. Benabed, J.-P. Bernard, M. Bersanelli, P. Bielewicz, J. J. Bock, J. R. Bond, J. Borrill, F. R. Bouchet, F. Boulanger, M. Bucher, C. Burigana, R. C. Butler, E. Calabrese, and e. a. Cardoso, Planck2018 results: Vi. cosmological parameters, Astronomy amp; Astrophysics **641**, A6 (2020).

[31] Z. Haiman, A. A. Thoul, and A. Loeb, Cosmological formation of low-mass objects, The Astrophysical Journal **464**, 523 (1996).

[32] T. Abel, G. L. Bryan, and M. L. Norman, The formation of the first star in the universe, Science **295**, 93–98 (2002).

[33] J. L. Johnson, T. H. Greif, and V. Bromm, Local radiative feedback in the formation of the first protogalaxies, The Astrophysical Journal **665**, 85–95 (2007).

[34] B. W. Keller, F. Munshi, M. Trebitsch, and M. Tremmel, Can cosmological simulations reproduce the spectroscopically confirmed galaxies seen at z 10?, The Astrophysical Journal Letters **943**, L28 (2023).

[35] H. Yajima, M. Abe, H. Fukushima, Y. Ono, Y. Harikane, M. Ouchi, T. Hashimoto, and S. Khochfar, Forever22: the first bright galaxies with population iii stars at redshifts $z \simeq 10-20$ and comparisons with jwst data (2023), arXiv:2211.12970 [astro-ph.GA].

[36] A. D. Goulding, J. E. Greene, D. J. Setton, I. Labbe, R. Bezanson, T. B. Miller, H. Atek, A. Bogdan, G. Brammer, I. Chemerynska, S. E. Cutler, P. Dayal, Y. Fudamoto, S. Fujimoto, L. J. Furtak, V. Kokorev, G. Khullar, J. Leja, D. Marchesini, P. Natarajan, E. Nelson, P. A. Oesch, R. Pan, C. Papovich, S. H. Price, P. van Dokkum, B. Wang, J. R. Weaver, K. E. Whitaker, and A. Zitrin, Uncover: The growth of the first massive black holes from jwst/nirspec – spectroscopic redshift confirmation of an x-ray luminous agn at z=10.1 (2023), arXiv:2308.02750 [astro-ph.GA].

[37] J. Yang, F. Wang, X. Fan, J. F. Hennawi, F. B. Davies, M. Yue, E. Banados, X.-B. Wu, B. Venemans, A. J. Barth, F. Bian, K. Boutsia, R. Decarli, E. P. Farina, R. Green, L. Jiang, J.-T. Li, C. Mazzucchelli, and F. Walter, Pōniuā'ena: A luminous z = 7.5 quasar hosting a 1.5 billion solar mass black hole, The Astrophysical Journal Letters **897**, L14 (2020).

[38] X. Yang and A. Li, Light from cosmic dawn hints at how interstellar dust is made, Nature **621**, 260 (2023).

[39] J. J. Eldridge, E. R. Stanway, L. Xiao, L. A. S. McClelland, G. Taylor, M. Ng, S. M. L. Greis, and J. C. Bray, Binary population and spectral synthesis version 2.1: Construction, observational verification, and new results, Publications of the Astronomical Society of Australia **34**, 10.1017/pasa.2017.51 (2017).

[40] F. Kirchschlager, F. D. Schmidt, M. J. Barlow, E. L. Fogerty, A. Bevan, and F. D. Priestley, Dust survival rates in clumps passing through the cas a reverse shock – i. results for a range of clump densities, Monthly Notices of the Royal Astronomical Society **489**, 4465–4496 (2019).

[41] F. Melia, The cosmic equation of state, Astrophysics and Space Science **356**, 393–398 (2014).

[42] C. L. Bennett, D. Larson, J. L. Weiland, N. Jarosik, G. Hinshaw, N. Odegard, K. M. Smith, R. S. Hill, B. Gold, M. Halpern, E. Komatsu, M. R. Nolta, L. Page, D. N. Spergel, E. Wollack, J. Dunkley, A. Kogut, M. Limon, S. S. Meyer, G. S. Tucker, and E. L. Wright, Nine-year Wilkinson Microwave Anisotropy Probe (WMAP) Observations: Final Maps and Results, ApJS **208**, 20 (2013), arXiv:1212.5225 [astro-ph.CO].

[43] P. A. R. Ade, N. Aghanim, M. I. R. Alves, C. Armitage-Caplan, M. Arnaud, M. Ashdown, F. Atrio-Barandela, J. Aumont, H. Aussel, C. Baccigalupi, A. J. Banday, R. B. Barreiro, R. Barrena, M. Bartelmann, J. G. Bartlett, N. Bartolo, S. Basak, E. Battaner, R. Battye, K. Benabed, A. Benoît, A. Benoit-Lévy, J.-P. Bernard, M. Bersanelli, B. Bertincourt, M. Bethermin, P. Bielewicz, I. Bikmaev, A. Blanchard, J. Bobin, J. J. Bock, H. Böhringer, A. Bonaldi, L. Bonavera, J. R. Bond, J. Borrill, F. R. Bouchet, and e. a. Boulanger, Planck2013 results. i. overview of products and scientific results, Astronomy amp; Astrophysics **571**, A1 (2014).

[44] A. Melchiorri, L. Mersini, C. J. Ödman, and M. Trodden, The state of the dark energy equation of state, Phys. Rev. D **68**, 043509 (2003).

[45] G. F. Lewis, Matter matters: unphysical properties of the r h= ct universe, Monthly Notices of the Royal Astronomical Society **432**, 2324 (2013).

[46] F. Melia, High-z quasars in the rh= ct universe, The Astrophysical Journal **764**, 72 (2013).

[47] Y. Gong and A. Wang, Energy conditions and current acceleration of the universe, Physics Letters B **652**, 63 (2007).

[48] Y. Gong, A. Wang, Q. Wu, and Y.-Z. Zhang, Direct evidence of acceleration from a distance modulus–redshift graph, Journal of Cosmology and Astroparticle Physics **2007** (08), 018.

[49] A. G. Riess, S. A. Rodney, D. M. Scolnic, D. L. Shafer, L.-G. Strolger, H. C. Ferguson, M. Postman, O. Graur, D. Maoz, S. W. Jha, B. Mobasher, S. Casertano, B. Hayden, A. Molino, J. Hjorth, P. M. Garnavich, D. O. Jones, R. P. Kirshner, A. M. Koekemoer, N. A. Grogin, G. Brammer, S. Hemmati, M. Dickinson, P. M. Challis, S. Wolff, K. I. Clubb, A. V. Filippenko, H. Nayyeri, U. Vivian, D. C. Koo, S. M. Faber, D. Kocevski, L. Bradley, and D. Coe, Type ia supernova distances at redshift gt;1.5 from the hubble space telescope multicycle treasury programs: The early expansion rate, The Astrophysical Journal **853**, 126 (2018).

[50] M. Bilicki and M. Seikel, We do not live in the rh = ct universe: We do not live in the rh = ct universe, Monthly Notices of the Royal Astronomical Society **425**, 1664–1668 (2012).

[51] P. van Oirschot, J. Kwan, and G. F. Lewis, Through the looking glass: why the 'cosmic horizon' is not a horizon, Monthly Notices of the Royal Astronomical Society 10.1111/j.1365-2966.2010.16398.x (2010).

[52] F. Melia, The anomalous 21-cm absorption at high redshifts, The European Physical Journal C **81**, 10.1140/epjc/s10052-021-09029-4 (2021).